Journal of Power Sources 214 (2012) 75–83

Contents lists available at SciVerse ScienceDirect

Journal of Power Sources

journal homepage: www.elsevier.com/locate/jpowsour

Structure and high temperature physical properties of glass seal materials in solid oxide electrolysis cell

Jie Hao [a,b], Qingfeng Zan [a,b,*], Desheng Ai [a,b], Jingtao Ma [a,b], Changsheng Deng [a,b], Jingming Xu [b]

[a] State Key Lab of New Ceramics and Fine Processing, Tsinghua University, Beijing 100084, PR China
[b] Institute of Nuclear and New Energy Technology, Tsinghua University, Beijing 100084, PR China

ARTICLE INFO

Article history:
Received 22 March 2012
Accepted 23 March 2012
Available online 21 April 2012

Keywords:
Solid oxide electrolyzes/fuel cells
Glass-ceramic
Wetting ability
Thermal expansion coefficient
Stability
Infrared spectra

ABSTRACT

Three series of $BaO-CaO-SiO_2-Al_2O_3$, $SrO-SiO_2-Al_2O_3$, and $SrO-CaO-SiO_2-Al_2O_3$ glasses are prepared. Their basic physical properties are measured using dilatometry and differential scanning calorimetry from room temperature to the softening temperature. Their structures are characterized with infrared spectroscopy. The wetting characteristics of all glasses are examined by monitoring the change in shape of a cube specimen on crofer22 substrates from room temperature to flow temperature with a high temperature shape microscope. Five main absorption bands can be distinguished in the infrared absorption spectra of the three systems. The optimum ranges of sealing temperature of the glasses are determined. The $24SrO-16CaO-25SiO_2-8Al_2O_3$ glass is found to be the best sealant for the solid oxide electrolyzer/fuel cells under low loading without leakage. SrO improves the wetting ability of the glass by decreasing the contact angle between the glass and crofer22 substrates. The thermal properties of all the glasses fulfill the requirements for sealing solid oxide electrolysis/fuel cells. In terms of air tightness, the SrO-containing glass shows the best wetting ability among other glasses, and is the most suitable sealant for planar solid oxide electrolyzers/fuel cells.

1. Introduction

Energy and environmental issues have gained the attention of many countries throughout the world in recent years. Non-renewable energy resource depletion and the greenhouse gas effect have forced countries to actively improve their energy efficiency. Solid oxide electrolysis/fuel cells (SOECs/SOFCs) have been actively studied, either as H_2-producing devices (SOECs) or clean and efficient energy conversion devices (SOFCs). However, many technical problems must be solved for commercial applications. In planar SOECs/SOFCs (p-SOECs or p-SOFCs), gas-tight sealing is a basic requirement in preventing gases from mixing in the anode and the cathode, and in providing electrical insulation to avoid shunting. Hence, the coefficients of thermal expansion (CTEs) of the sealants must match those of other cell components, such as the interconnect [$(12–14) \times 10^{-6}$ K^{-1}] and electrolyte [$(10–12) \times 10^{6}$ K^{-1}] [1–3]. In addition, the seals must fulfill chemical requirements. They must be chemically compatible with other components and stable in oxidizing, reducing, or oxidizing–reducing atmospheres.

Many glasses and glass-ceramics have been used as sealants in p-SOECs or p-SOFCs [4–6]. In those materials, $BaO-CaO-SiO_2-Al_2O_3$-based (BCSA) [7,8], $SrO-SiO_2-Al_2O_3$-based (SSA) [9,10], and $SrO-CaO-SiO_2-Al_2O_3$-based (SCSA) sealing glasses [11,12] have shown excellent sealing performances. Their basic properties have been widely studied, including CTE, glass transition temperature (T_g), glass softening temperature (T_s), and interface reactions between seals and the interconnect. These materials have also exhibited good chemical and thermal stability after running for thousands of hours at their working temperature in planar SOEC/SOFC systems. As additives to glasses, each substance has specific effects on glass. For example, alkaline earth oxide has a strong influence on T_s and T_g in the glass [4,13]. Alumina acts as a crystallization agent in the glass [4]. A small amount of boron oxide B_2O_3, a lower-temperature glass former, can be used to reduce the viscosity of glasses and improve the wetting ability [4]. In addition, La_2O_3 has been used as a viscosity modifier and long-term CTE stabilizer [4]. However, glass composition has

* Corresponding author. Beijing Key Lab of Fine Ceramics, Tsinghua University, Beijing 100084, PR China. Tel.: +86 10 89796112; fax: +86 10 89796105.
E-mail address: zanqf@tsinghua.edu.cn (Q. Zan).

0378-7753/$ – see front matter © 2012 Elsevier B.V. All rights reserved.
doi:10.1016/j.jpowsour.2012.03.087

a significant influence on glass structure, and the glass structure determines the properties of glass. Some reports have presented in-depth reports correlating the basic high temperature physical properties with the structure of the glasses.

Infrared spectra of glasses can sensitively probe into the local structure of silicate glasses [14–18]. The amount of non-bridging oxygen (NBO) in a silicate system can be reflected by the intensity of relevant infrared absorption spectra [16]. In the current work, the structure, particularly, the amount of NBO of three glass-ceramic sealing materials, i.e., BCSA-based, SSA-based seal, and SCSA-based seal glasses used in SOECs/SOFCs, have been studied by infrared spectroscopy and correlated with the basic physical properties of the glasses. The changes in the physical shapes of the glasses as well as their wetting abilities from room temperature to melting temperatures were also investigated to determine their sealing temperatures.

2. Experimental

2.1. Glass preparation

BCSA-based, SSA-based, and SCSA-based seal glasses were chosen as the starting points for glass composition because of their good glass-forming properties, chemical stability and thermal stability, and high CTEs. The raw materials of these three glasses are presented in Table 1. In Table 1, the M/F is the molar ratio of the glass modifier to the glass former. The constituents of CaO, BaO, Al_2O_3, B_2O_3, La_2O_3, and SiO_2 were in analytical grade (Zhongguancun Chemical Company, Beijing, China). All of the glasses were prepared by melting thoroughly blended constituent compounds in a platinum crucible at 1500 °C for 2 h under static air. Afterward, the glass melts were poured into a graphite die, cooled, and then annealed in air for 3 h–4 h to eliminate residual thermal stresses.

2.2. Characterization

Fourier transform infrared spectroscopy (FTIR, Nicolet 6700FTIR, USA) in the range of 400 cm^{-1} to 1800 cm^{-1} was used to study the structure and phase morphology of unconstrained glass samples. The amount of NBO has a certain impact on the infrared spectra of glasses.

Annealed glasses were then cut into rectangular blocks of 5 mm × 5 mm × 25 mm for measurement their CTEs. The CTEs of as-cast glasses were measured with a dilatometer (DIL 402C, Nietzsche, Germany) from room temperature to the softening temperature of each glass with bars of 5 mm × 5 mm × 25 mm, at a heating rate of 20 °C min^{-1}. From the thermal expansion curves of the glasses, the softening temperature and the average CTEs of each as-cast glass were obtained. The thermal properties of glass powders were characterized with a differential scanning calorimeter (DSC204, Nietzsche, Germany) and then calibrated using the melting points of high purity indium and zinc. The non-isothermal experiments were performed by heating approximately 30 mg of the sample in Pt crucibles in oxidizing atmosphere, with an empty Pt crucible as the reference. A heating rate of 20 °C min^{-1} was employed in the range 25 °C–1000 °C, after which T_g and T_c were obtained from the DSC curves of the glasses.

Glasses were cut into rectangular blocks of 3 mm × 3 mm × 3 mm to observe the changes in the physical shape and wetting abilities of the glasses from room temperature to melting temperature. The physical shape and wetting ability were observed with a high temperature optical microscope (RDS-04, Northeastern University, China). The specimens were placed in a static air box furnace fitted with a quartz door. The wetting characteristics of all glasses were examined by monitoring the change in shape of the specimens on crofer22 APU (Thyssen-Krupp, Germany) substrates from room temperature to melting temperature with a heating rate of 20 °C min^{-1}. A high-speed video camera with a zoom lens was used to record the changes in the physical shapes and wetting abilities of the glasses.

Table 1
Glass compositions (by mol%).

Glass No.	Series	BaO	SrO	CaO	SiO_2	B_2O_3	Al_2O_3+La_2O_3	*M*/*F*	Si/B
G1	BCSA	20	0	20	36	12	12	0.83	3
G2		24	0	16	34.3	13.7	12	0.83	2.5
G3		24	0	16	32	16	12	0.83	2
G4		20	0	20	24	24	12	0.83	1
G5		16	0	16	42	14	12	0.57	3
G6		16	0	16	28	28	12	0.57	1
G7		28	0	16	30	15	11	0.97	2
G8		24	0	24	30	10	12	1.20	3
G9	SSA	0	36	0	41	13	10	0.66	3
G10		0	40	0	33	17	10	0.80	2
G11		0	40	0	25	25	10	0.80	1
G12		0	44	0	30	16	10	0.95	2
G13	SCSA	0	16	16	43	15	10	0.55	3
G14		0	24	16	33	17	10	0.80	2
G15		0	28	16	31	15	10	0.96	2
G16		0	24	16	25	25	10	0.80	1

3. Results

3.1. Non-bridging oxygen

The composition of the glass determines its structure and the amount of NBO. However, understanding the structure of glass and quantifying the NBO are difficult tasks, especially for those containing B_2O_3 and Al_2O_3. The cations of intermediate Al_2O_3 have a higher valance and lower coordination number [19,20]. They may or may not participate in the glass network. According to Stevel's glass network theory [21], on one hand, the intermediate oxide Al_2O_3 act as a glass intermediate when the contents of alumina exceed those of the alkaline earth oxides. On the other hand, the intermediate oxide Al_2O_3 act as a glass network former if the contents of alkaline earth oxides exceed those of alumina. In borate glass, boron oxide has two forms: BO_3 (trigonal boron species) and BO_4 (tetrahedral boron species). In this glass the alkaline earth oxides may have converted the boroxyl groups (trigonal boron species) into three-dimensional (3D) borate groups (tetrahedral boron species). If the content of alkaline earth oxides exceeds 30 mol%, the boroxyl groups (trigonal boron species) disappear [19].

In Table 1, the contents of alkaline earth oxides exceed 30 mol% in all glasses. Hence, most of the BO_3 transform into BO_4, and the Al_2O_3 oxides act as the glass network former. According to Stevel's glass network theory, the number of NBO(X) can be calculated using Equation (1) below:

$$X = \frac{2\sum O_{\text{NetworkFormer+Modifier}}}{\sum F_{\text{NetworkFormer}}} - 4 \quad (1)$$

where F is the number of glass network former atoms, i.e., Si, B, and Al; and O is the number of all oxygen atoms in each glass. The results are given in Table 2 below.

Table 2
The number of NBO(X) in all glasses.

BCSA				SSA		SCSA	
No.	X	No.	X	No.	X	No.	X
G1	0.52	G5	0.23	G9	0.34	G13	0.24
G2	0.45	G6	0.32	G10	0.38	G14	0.39
G3	0.40	G7	0.91	G11	0.17	G15	0.91
G4	0.18	G8	0.90	G12	0.43	G16	0.19

3.2. Infrared absorption spectra

In the present systems, the silicate units with four, three, two, one, and zero bridging oxygen atoms are denoted as Q^4, Q^3, Q^2, Q^1 and Q^0, respectively [19]. The infrared absorption spectra of three seal materials are presented in Figs. 1–4, respectively. From Figs. 1–4, 5 main absorption bands can be distinguished: 440 cm^{-1}–530 cm^{-1}, which is attributed to the bending vibration of Si–O–Si in SiO_4 unit; 700 cm^{-1}–750 cm^{-1} attributed to the bending vibration of B–O–B linkages in BO_4 unit; and 850 cm^{-1}–1150 cm^{-1} attributed to the stretching vibration of Si–O–Si linkages in SiO_4 unit. The band at 850 cm^{-1}–1150 cm^{-1} has also been observed in the Raman spectra [16,17]. The 850 cm^{-1}–1150 cm^{-1} absorption band may also contain 4 sub-absorption bands: 1060 cm^{-1}–1105 cm^{-1} (from the Q^3 units), 949 cm^{-1}–1010 cm^{-1} (from the Q^2 units), ~917 cm^{-1} (from the Q^1 units), and ~872 cm^{-1} (from the Q^0 units). For the band at 1170 cm^{-1}–1250 cm^{-1}, some reports [22] suggested that this is attributed to the stretching vibration of B–O–B linkages in the $B_2O_5^{4-}$ unit, whereas some other reports [23,24] reported that it is attributed to the stretching vibration of Q^4, because the Q^4 groups exhibit additional features in this region. The high frequency band at 1300 cm^{-1}–1400 cm^{-1} is attributed to the stretching vibration of the B–O ring bonds of the borate groups.

In the BCSA system (Figs. 1 and 2), with the decrease of the ratio of Si/B, the peak of the 440 cm^{-1}–530 cm^{-1} absorption band shifts to a higher frequency from 491 cm^{-1} to 495 cm^{-1}. Thus, there is more difficulty in the bending vibration of Si–O–Si linkages with a decrease in the amount of NBO. The peak of the 700 cm^{-1}–750 cm^{-1} absorption band also shifts to a higher frequency, from 723 cm^{-1} to 728 cm^{-1}, although this did not appear in the infrared absorption spectra of glass G1. Moreover, with the decrease of the ratio of Si/B, the band becomes sharper. Hereby, when contents of B_2O_3 are low in the BCSA glass system, B exists in the BO_3 units. With the increase of B_2O_3 content, the BO_3 units convert into BO_4 units. The peak of the 850 cm^{-1}–1150 cm^{-1} absorption band also shifts to a higher frequency from 959 cm^{-1} to 978 cm^{-1}. As mentioned earlier, the 850 cm^{-1}–1150 cm^{-1} absorption band contains 4 sub-absorption bands: 1060 cm^{-1}–1105 cm^{-1} (Q^3 units), 949 cm^{-1}–1010 cm^{-1} (Q^2 units), ~917 cm^{-1} (Q^1 units), and ~872 cm^{-1} (Q^0 units). The band shifts to a high frequency mean, such that the contents of the Q^2 and Q^3 units increase with the decrease of the amount of NBO from 0.52 to 0.18. This indicates that the silicate units exist mainly with three bridging oxygen atoms, when the amount of NBO is very small. Table 2 shows that from G1 to G4, the amount of NBO decreases suddenly, but the width of this absorption band decreases steadily. Thus, 1170 cm^{-1}–1250 cm^{-1} may be attributed to the stretching vibration of B–O–B linkages in $B_2O_5^{4-}$ unit or the stretching vibration of Q^4. SiO_2 is the main glass network former in the glass series, and the contents of SiO_2 are 24%–36% (mol%); thus, SiO_4 units must exist in all kinds of glass, because the 1170 cm^{-1}–1250 cm^{-1} absorption band is the stretching vibration of B–O–B linkages in the $B_2O_5^{4-}$ units. In the infrared absorption spectra of G5 and G6, however, no absorption band is observed in the 1170 cm^{-1}–1250 cm^{-1} band. All these evidence suggest that 1170 cm^{-1}–1250 cm^{-1} is indeed the

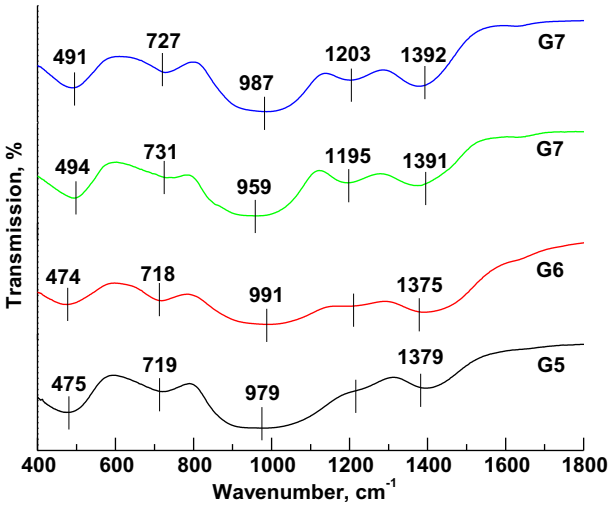

Fig. 2. The infrared absorption spectra of G5–G8.

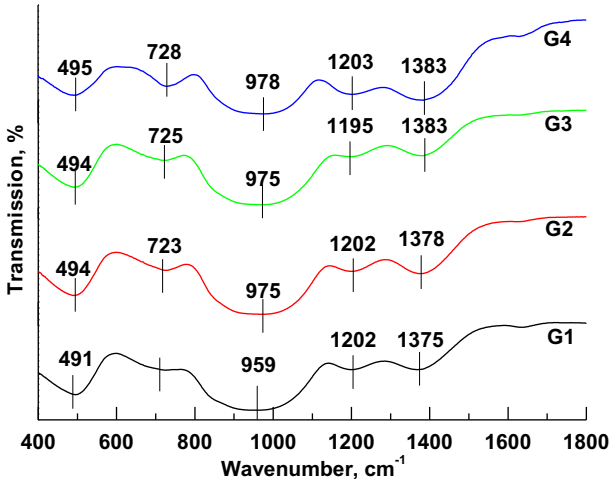

Fig. 1. The infrared absorption spectra of G1–G4.

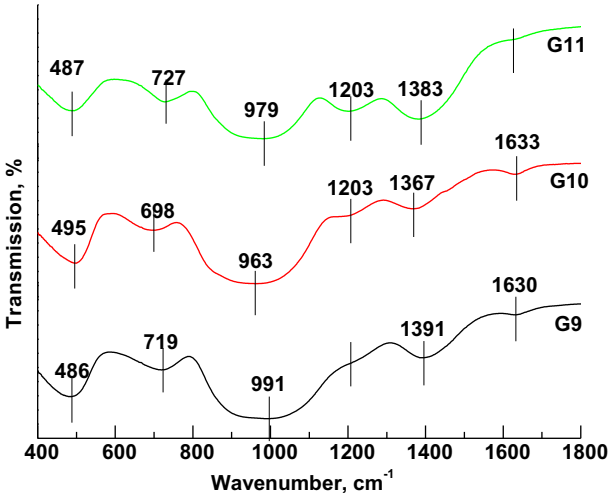

Fig. 3. The infrared absorption spectra of G9–G11.

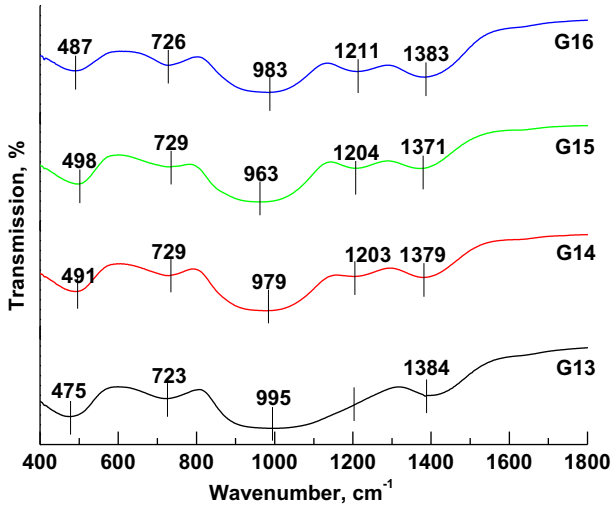

Fig. 4. The infrared absorption spectra of G13–G16.

stretching vibration of B–O–B linkages in $B_2O_5^{4-}$ units. From Figs. 1and 2, with the decrease of the ratio of Si/B, the 1170 cm^{-1}–1250 cm^{-1} absorption band steadily become sharper. An anomalous phenomenon is detected in the spectra of G6: when the B_2O_3 content reaches 28% (mol%), the 1170 cm^{-1}–1250 cm^{-1} absorption bands disappear. The reason for this has been postulated in previous studies [16], and is known as the "boron anomaly." Another possibility is the effect of combined ions, which may change the overall network structure [4].

The SSA system (Fig. 3) is different from the BCSA system. With the decrease of the ratio of Si/B, the peak of the 440 cm^{-1}–530 cm^{-1} absorption band shifts to a higher frequency from 486 cm^{-1} to 495 cm^{-1} and then goes down to 487 cm^{-1}. On the contrary, the peak of the 700 cm^{-1}–750 cm^{-1} absorption band shifts to a lower frequency and then increases from 719 cm^{-1} to 698 cm^{-1} and then to 727 cm^{-1}. Given the decrease of the ratio of Si/B, the peak also becomes sharper. The relative intensity of the BO_3 bands indicates a relative ratio of BO_3 to BO_4 [17]. The change trend of the 850 cm^{-1}–1150 cm^{-1} band is similar to the 700 cm^{-1}–750 cm^{-1} absorption bands, but the half-height width of this absorption band decreases significantly. The band shift to higher frequency means that the contents of the Q^2 and Q^3 units increase with the decrease of the ratio of Si/B. As to the 1170 cm^{-1}–1250 cm^{-1} absorption band, it steadily becomes sharper with the decrease of ratio of Si/B. A notable result is that a high frequency absorption band appears in 1590 cm^{-1}–1680 cm^{-1}, which has not been found in published data. The band is tentatively assigned to metaborate units and localized stretching vibration modes of the B–O^- bonds. However, further experiments are needed to clarify its significance.

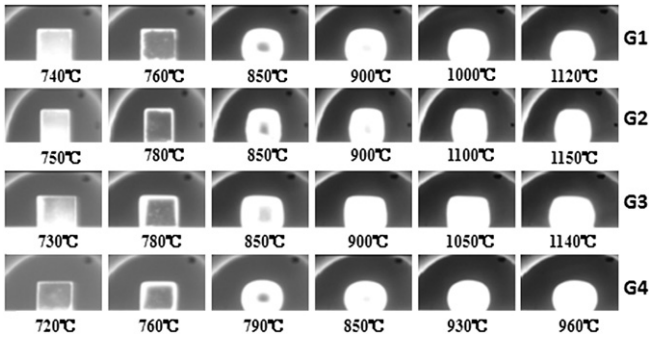

Fig. 5. Shape changes of the cube specimens (3 mm × 3 mm × 3 mm) with increasing temperature for G1–G4 (heating rate of 20 °C min^{-1}).

Fig. 4 illustrates the infrared absorption spectra of the SCSA glass system. SCSA glasses are similar in composition to BCSA glasses, with only BaO being replaced by SrO. In the SCSA glass system, the change trend of the infrared absorption spectra is similar to that of BCSA glasses. The only difference is that these five absorption bands experience small fluctuations with changes in bond energy.

Based on the above results, discrepancies with prior reports are observed in the infrared absorption spectra of three series glasses. First, with the increase of B_2O_3, the peak of the 850 cm^{-1}–1150 cm^{-1} absorption band shifts a higher frequency because of the increase of the contents of Q^3 and Q^2. In the glass structure, Q^1 and Q^0 are very unstable, but Q^4 is stable. Along with the increase of B_2O_3, the interconnectivity of glass structure increases. Then Q^1 and Q^0 convert into Q^3 or Q^2 with the co-top form or co-edge form, after which the island structure of silicon-oxygen tetrahedron simultaneously transforms into the frame or chain structure. Thus, the peak of the 850 cm^{-1}–1150 cm^{-1} absorption band shifts to a higher frequency and concentrates on the 1060 cm^{-1}–1105 cm^{-1} (Q^3 units) and 949 cm^{-1}–1010 cm^{-1} (Q^2 units) bands with the increase of the alkaline earth metal oxide content and silicon-oxygen ratio R. Second, in the three glass system, the 1590 cm^{-1}–1680 cm^{-1} absorption band of metaborate units changes significantly. In the SCSA and BCSA glasses, the absorption band almost does not appear. Rather, the microsoft absorption peaks are only present in the G1, G4, G7, and G8. However, in the SSA glasses, the absorption band has to be significantly enhanced. This phenomenon indicates that the metaborate content increases significantly. The above situation is likely caused by the "effect of combined ions" [25]. In this so-called effect, the glass structure or properties change in favor of the direction opposite to the scheduled performance with the increase in the types of the network modifier cation; this is due to the mutual interaction between the different types of network modification cations. When Sr^{2+}, Ba^{2+}, and Ca^{2+} ions exist alone, the field strength of the cation can bend two-dimensional space BO_3 into a 3D tetrahedral structure of the metaborate. When another cation or several ones are added to the borosilicate glass, the "effect of combined ions" weakens the attraction of the cation to the oxygen ions, thereby leading to the decrease of the tetrahedral structure BO_4. Thus, the disappearance or reduction of metaborate occurs in the SCSA glass systems and the BCSA glass system.

The glass structure change inevitably causes changes in the basic physical properties of glass. Such property changes are discussed in detail in the next chapter.

3.3. DSC of glasses

Based on the DSC curves, the crystallization temperatures of the glasses could be are obtained and presented in Table 3. In the BCSA system, while the constant ratio of M/F is 0.83 (M is the content of glass network modifier, F is the content of glass network former),

Table 3
Crystallization temperature of all kinds of glass.

BCSA				SSA		SCSA	
No.	T_c (°C)	No.	T_c (°C)	No.	T_c (°C)	No.	T_c (°C)
G1	706	G5	709	G9	765	G13	745
G2	696	G6	701	G10	752	G14	740
G3	672	G7	655	G11	700	G15	737
G4	663	G8	713	G12	–	G16	661

with the decrease of the ratio of Si/B from 3 to 1 (Si/B is ratio of the SiO_2 content to the B_2O_3 content in glass), the T_c of glass steadily decreases from 706 °C to 663 °C. Along with the increase of the ratio of M/F from 0.52 to 1.2, the T_c of glass also decreases from 709 °C to 655 °C, except for G8. The results indicate that B_2O_3 significantly reduces the crystallization temperatures of glass, whereas the alkaline earth oxides only weakly affect the T_c of glass.

In the SSA and SCSA systems, the same trend is also found. Along with the decrease of the ratio of Si/B from 3 to 1 and the stable ratio of $M/F = 0.83$, the T_c of glass steadily decreases from 765 °C to 700 °C in the SSA system, and from 745 °C to 661 °C in the SCSA system. However, a significant difference exists between the two systems, in that the T_c of the SSA glass is higher than that of the SCSA glass and is also higher than that of the BCSA glass. The T_c of seal glass having alkaline earth oxide increases in the order BaO < SrO < CaO < MgO. Field strength can increase the activation energy of atomistic migration in glass structure, thus reducing the frequency of structural transitions. In turn, this leads to a lower mobility of alkaline earth ions in the glass network system.

3.4. Coefficient of thermal expansion and softening temperature

The CTE of seal glass is one of the most important thermal properties for SOECs/SOFCs and should match those of other SOFC/SOEC components to avoid thermal stresses. The stresses can cause structural damage and performance degradation in the cell system. Usually, the CTEs of the interconnect in SOECs/SOFCs vary between 12.0×10^{-6} K^{-1} and 14.0×10^{-6} K^{-1} [19,20], and the CTEs of electrolytes vary between 10.0×10^{-6} K^{-1} and 12.0×10^{-6} K^{-1}. In practice, CTEs ranging from 10.0×10^{-6} K^{-1} to 12.0×10^{-6} K^{-1} is considered ideal for SOFC/SOEC applications, since under this condition, the thermal stress is smaller than the strength of the glass, and the cell can work stably at high temperatures.

The CTEs of all kinds of seal glass are measured from room temperature (T_R) to glass transition (T_g) and are presented in Table 4. In the BCSA system, the average CTE from T_R to T_S (softening temperature) are listed in Table 4. The T_S has an opposite trend of change to the CTEs in the four glasses. When the T_S reach the maximum, the CTE reaches the minimum. For G1, G2, G3 and G4, with the decrease of the ratio of Si/B from 3 to 1 and stable ratio of $M/F = 0.83$, the CTE of glass increases from 10.13×10^{-6} K^{-1} to 11.28×10^{-6} K^{-1}, but the T_S of glass steadily decreases from 678 °C to 645 °C. SiO_2 decreases CTE, and the contents of B_2O_3 need to be increased if a high CTE has to be achieved by glass formers.

The CTEs of G5, G6, G7, and G8, as well as the average CTEs from T_R to T_S are listed in Table 4. The T_S of the glasses are 752 °C, 658 °C, 651 °C and 664 °C, respectively. Given the increase of the ratio of M/F from 0.57 to 1.20, the CTE of glass increases from 9.25×10^{-6} K^{-1} to 11.17×10^{-6} K^{-1} except for G6. The Si/B ratio for G6 is unity, and the B_2O_3 content reaches 24 mol%. The CTE of G6 is greater than that of G7, although the content of alkaline earth oxides in G7 is higher than that of G6. Hence, the effect of B_2O_3 in increasing CTE is greater than that of the alkaline earth oxides.

The SSA system is similar to the BCSA system. Given the decrease of the ratio of Si/B, the CTEs of G9, G10, and G11 increase from 9.72×10^{-6} K^{-1} and 10.59×10^{-6} K^{-1} to 10.67×10^{-6} K^{-1}, and the T_S of the three glasses decrease from 781 °C and 751 °C to 684 °C. Compared with G1, G3 and G4, the increase of the CTE of the SSA system glass is smaller than that of the BCSA glasses with the increase of alkaline earth oxide content. The CTE increases directly with the field strength of alkaline earth cations in the order $Sr^{2+} < Ba^{2+} < Ca^{2+}$ due to the weaker bonding at lower field. T_S changes in the same trend. Hence, the effect of the network modifier on the CTE and T_S of a seal glass is complex and is related to the field strength and quantity of a network modifier.

The SCSA glass system is similar in composition with the BCSA glass system, with only BaO being replaced by SrO. In the SCSA glass system (Table 4), the change of CTE is similar to that of BCSA glasses. The average CTEs from T_R to T_S for G1, G2, G3, and G4 are 9.77×10^{-6} K^{-1}, 10.12×10^{-6} K^{-1}, 10.59×10^{-6} K^{-1} and 10.87×10^{-6} K^{-1}, respectively. The T_S values of G13 to G16 are 686 °C, 655 °C, 737 °C and 656 °C, respectively. An anomalous phenomenon is observed in G15, the T_S of which is the highest in the SCSA glasses. In this case, the connectivity theory of Lu K. et al. is insufficient in explaining this phenomenon [4]. The CTE of materials is closely related to the properties of bonding and bond energy between the anions and the cations. In turn, these are also closely related to the field strength of cations of the glass network modifier and former as well as to ionic radius. The relation between the CTE and efficiency of field strength is discussed in detail in a later section.

In the BCSA system, with the decrease of the ratio of Si/B from 3 to 1 and the stable ratio of $M/F = 0.83$, the CTE of glass increases from 10.13×10^{-6} K^{-1} to 11.28×10^{-6} K^{-1}, and the T_S of glass steadily decreases from 678 °C to 645 °C. The B_2O_3 causes a greater increase of the CTE than do alkaline earth oxides. In the SSA and SCSA systems, the changes of CTEs are similar to those observed in the BCSA system. The CTEs also increase directly with the field strength of alkaline earth cations in the order $Sr^{2+} < Ba^{2+} < Ca^{2+}$. Their T_S changes show the same trend. The relationship between CTE and the total contents of alkaline earth oxides and B_2O_3 is clear, that is, the CTE of glass increases with the contents of alkaline earth oxides and B_2O_3; this increasing trend slows down steadily. Therefore, the CTE can be estimated using the total alkaline earth oxide and B_2O_3 content.

3.5. Shape evolution and contact angle at high temperature

The wetting characteristics of all glasses were examined by monitoring the change in shape of a cube specimen on crofer22 substrates from room temperature to melting temperature with a heating rate of 20 °C min^{-1}. A typical series of photographs showing the evolution of all glass during heating without additional pressure are presented in Figs. 5–8.

In the BCSA system (Fig. 5), the starting sintering temperature ($T_{sintering}$, at which temperature glass starts to sinter and its rough surface becomes smooth) of G1 is ~740 °C, melting temperature

Table 4
The T_s and CTEs of all glasses.

BCSA						SSA			SCSA		
No.	T_s (°C)	CTE (10^{-6} K^{-1})	No.	T_s (°C)	CTE (10^{-6} K^{-1})	No.	T_s (°C)	CTE (10^{-6} K^{-1})	No.	T_s (°C)	CTE (10^{-6} K^{-1})
G1	678	10.13	G5	752	9.23	G9	781	9.72	G13	686	9.77
G2	670	10.46	G6	658	10.85	G10	751	10.59	G14	655	10.12
G3	655	10.55	G7	651	10.67	G11	684	10.67	G15	637	10.59
G4	645	11.28	G8	664	11.17	G12	–		G16	656	10.87

Note: The CTEs were measured within the range of T_r to T_g.

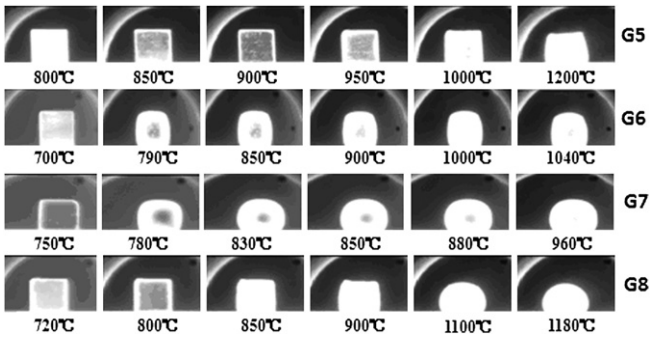

Fig. 6. Shape changes of the cube specimens (3 mm × 3 mm × 3 mm) with increasing temperature for G5–G8 (heating rate of 20 °C min^{-1}).

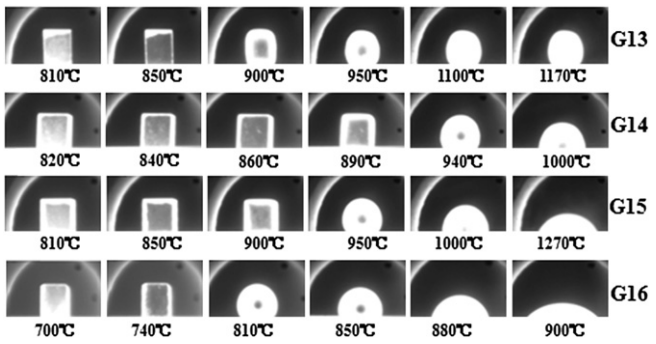

Fig. 8. Shape changes of the cube specimens (3 mm × 3 mm × 3 mm) with increasing temperature for G13–G16 (heating rate of 20 °C min^{-1}).

(T_m, at which temperature the viscosity of glass drops sharply) is 900 °C, and flowing temperature (T_f, at which temperature glass starts to flow liking a liquid) is 1120 °C. The shape change of glass sharply occurs between 760 °C and 800 °C; the temperature range in which the shape changes sharply is defined as maximum difference. In this range, the viscosity of the glass declines rapidly with increasing temperature, leading to rapid changes in the shape of the glass. For glass G1, from the shape at different temperatures, the optimum sealing temperature range is from 800 °C to 870 °C. In the scope of temperature, the glass is sticky stagnant, and under pressure, the glass exhibits viscous flow; moreover, the SOEC/SOFC stack is easier to seal without any leakage. The respective $T_{sintering}$, T_m, and T_f of sintering G2, G3, and G4 are listed in Table 5. The change of glass shape clearly occurs between at 780 °C–830 °C, 770 °C–820 °C and 730 °C–800 °C, respectively (Fig. 5). Therefore, the optimum sealing temperature ranges for G2, G3, and G4 are 820 °C–900 °C, 810 °C–870 °C and 780 °C–830 °C, respectively. With the decrease of the ratio of Si/B from 3 to 1, and at the stable ratio of M/F, 0.83, the $T_{sintering}$, T_m, and T_f of these glass decrease from 750 °C to 720 °C, 900 °C–850 °C and 1150 °C–960 °C, respectively. This indicates that the B_2O_3 can significantly change the physical properties of BCSA glasses. As for other systems, when the B_2O_3 contents reach 15% (mol%), an anomalous point occurs.

Based on Fig. 6, the $T_{sintering}$, T_m, and T_f of G5, G6, G7, and G8 are also listed in Table 5. Their optimum sealing temperature ranges are 950 °C–1050 °C, 850 °C–950 °C, 780 °C–830 °C and 830 °C–900 °C, respectively. Except for G8, with the increase of ratio of *M*/*F* from 0.57 to 1.20, the $T_{sintering}$, T_m, and T_f of G5, G6, and G7, decrease from 850 °C to 750 °C, 1100 °C to 880 °C and 1200 °C to 960 °C, respectively. This indicates that alkaline earth oxides also significantly change the physical properties of BCSA glasses. Nevertheless, this cannot explain the abnormal behavior of G8 as far as http://www.iciba.com/consideration/the ratio of Si/B is concerned. The B_2O_3 content cannot explain the abnormal phenomenon either. The relation between the $T_{sintering}$, T_m, and T_f on the one hand and the total quantity of B_2O_3 and alkaline earth oxides on the other is discussed in detail in a later section.

In the SSA system (Fig. 7), the $T_{sintering}$, T_m, and T_f of G9 are observed at ~850, 1100 and 1240 °C, respectively, and the maximum difference occurs between 900 °C and 1000 °C. Within the temperature range, the glass maintains a relatively high viscosity. Therefore, the optimum sealing temperature range of G9 is from 930 °C to 980 °C. In this temperature range, the glass is sticky stagnant, and as such, it could seal the SOEC/SOFC stack well even under pressure. The $T_{sintering}$, T_m, and T_f of G10 and G11 are listed in Table 5. The maximum difference occurs at 900 °C–950 °C and at 800 °C–850 °C (Fig. 7); therefore, their optimum sealing temperature ranges are 930 °C–980 °C and 800 °C–840 °C, respectively. Similar to the BCSA system, with the decrease of the ratio of Si/B from 3 to 1, the $T_{sintering}$, T_m, and T_f of these glasses decrease from 850 °C to 750 °C, 1100 °C–850 °C and 1240 °C–920 °C, respectively.

In the SCSA system (Fig. 8), the $T_{sintering}$, T_m, and T_f of G13 are ~830, 1000 and 1170 °C, respectively. The maximum difference occurs between 870 °C and 930 °C. Therefore, the optimum sealing temperature range of G9 is 880 °C–930 °C. In this temperature range, the glass can work well in an SOEC/SOFC stack. The respective $T_{sintering}$, T_m, and T_f of G14, G15, and G16 are listed in Table 4. Based on Fig. 8, the maximum difference occurs at 890 °C–940 °C, 900 °C–950 °C, and 770 °C–810 °C; thus, their optimum sealing temperature ranges are 900 °C–950 °C, 920 °C–960 °C and 760 °C–810 °C, respectively. Similar to the BCSA system, with the decrease of the ratio of Si/B from 3 to 1, all $T_{sintering}$, T_m, and T_f of this glass decrease. In addition, in G14, G15 and G16, no visible flowing temperature points occur at high temperatures.

Contact angles are known to vary with time and temperature [21]. The wetting ability of all glasses in BCSA, SSA, and SCSA systems are represented by the contact angles between the glasses and the crofer22 substrates at different temperatures. Different wetting abilities are observed among BCSA, SSA, and SCSA systems. G7, G11, and G16 are representatives of the three systems chosen

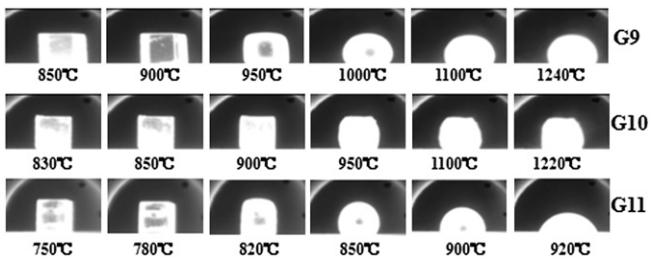

Fig. 7. Shape changes of the cube specimens (3 mm × 3 mm × 3 mm) with increasing temperature for G9–G11 (heating rate of 20 °C min^{-1}).

Table 5
The $T_{sintering}$, T_m, and T_f of all glass samples.

No.	G1	G2	G3	G4	G5	G6	G7	G8
$T_{sintering}$, °C	740	750	730	720	850	760	750	800
T_m, °C	900	900	870	850	1100	900	880	1050
T_f, °C	1120	1150	1140	960	1200	1040	960	1180
No.	G9	G10	G11	G12	G13	G14	G15	G16
$T_{sintering}$, °C	850	830	750		830	820	810	730
T_m, °C	1100	950	850		1000	960	950	840
T_f, °C	1240	1120	920		1170	1000	1270	900

Table 6
Contact angles of G7, G11, and G16 on the surface of crofer22 substrates at different temperatures.

G7		G11		G16	
Temperature (°C)	Contact angles (°)	Temperature (°C)	Contact angles (°)	Temperature (°C)	Contact angles (°)
800	126	820	114	800	123
820	129	840	122	820	119
840	131	860	117	840	110
860	120	880	113	860	90
880	118	900	92	880	68
960	107	920	68	900	46

for further study. Based on Figs. 5, 7 and 8, all the contact angles of the three systems of glass are measured and presented in Table 6. For G7, the melting point is ~840 °C, which is considered a turning point for its contact angle. Above 840 °C, the angles decrease and approach 107° at 960 °C, whereas below 840 °C, the angles increase gradually and reach a maximum of 131° at ~840 °C. Although the contact angle is larger than 130°, a suitable sealing between glass and interconnect can be achieved in practical operation, because the glass is expected to be under pressure from adjacent components or from the load of its own gravity. Along with the change of loading, the contact region and status may also change correspondingly. G7 adheres well to crofer22 substrates during the whole process and can avoid the glass spreading freely on the surface of crofer22 substrates at high temperature above the glass melting point. For G11, the true melting point is also ~840 °C (Table 6), which is a turning point from solid to liquid. Above 840 °C, the angles decrease and approach 68° at 920 °C, whereas below 840 °C, the angles increase gradually and reach a maximum of 122° at ~840 °C. Hence, for crofer22 substrates, the wetting ability of G11 is better than that of G7. G16 has a better wetting ability than G11. The true melting point of G16 is also ~800 °C as seen in Table 6, and so the contact angle at 800 °C is a turning point. Above 800 °C, the angles decrease and approach 46° at 900 °C, whereas below 800 °C, the angles increase gradually and reach a maximum of 123° at ~800 °C. With regards wetting ability, G16 may be the best option to seal the SOECs/SOFCs under low loading without leakage. The contact properties of G11 and G16 fulfill the requirement for sealing SOECs/SOFCs at mid-high temperature with good air tightness as well. Based on the analysis above, SrO can improve the wetting ability of glass by decreasing the contact angle between the glass and crofer22 substrates.

Based on the above results, the discrepancy of SrO with prior reports is also observed in three series glasses. Previous studies reported that SrO modifies glass properties, such as T_g, T_s and CTE, but it cannot affect the wetting ability of glass. As demonstrated in the current work, SrO can improve the wetting ability of glass by decreasing the contact angle between the glass and crofer22 substrates. However, the interfacial energy is determined by the surface tension of the melting glass. The field strength of Sr^{2+} is more powerful than that of Ba^{2+}, and so the attraction of Sr^{2+} to the surface of the oxygen ions is bigger than that of Ba^{2+}. Therefore, Sr^{2+} can reduce the surface tension of molten glass in the SSA and SCSA glass systems as well as reduce the interfacial energy between the molten glass and crofer22 substrates. The SrO can improve the wetting ability of glass by decreasing the contact angle between the glass and crofer22 substrates.

4. Discussion

4.1. The relations between NBO, compositions, and CTE

The relationships between the physical properties of glass and the composition of glass are very complicated. The composition of the glass determines the amount of NBO and the structure and properties of glass. The CTE of a seal glass depends on such factors as glass structure symmetry, bond-bending, molar-free volume, and so on. The BCSA system is relatively complete compared with the two other systems, and thus its relationships with NBO, compositions and T_s, and CTE are analyzed below. The relationship between NBO and CTE is shown in Fig. 9. A clear correlation between NBO and CTE cannot be seen, indicating a complex relationship between NBO and CTE. With a constant B_2O_3 content, the CTE of glass initially increases from 9.25×10^{-6} K^{-1} to 11.17×10^{-6} K^{-1}, with an increase of the number of NBO when the B_2O_3 content exceeds 20 mol%. However, this trend is not observed.

On the other hand, according to the previous analysis in Section 3.2, SiO_2 generally decreases CTE. Furthermore, the relationship between CTE and the total alkaline earth oxide and B_2O_3 contents (by mol%) clearly indicates that the CTE of glass increases with the increase of the total alkaline earth oxide and B_2O_3 content as show in Fig. 10 (where AO represents the alkaline earth oxides, BaO, and CaO). Therefore, the estimation of the CTE from the total alkaline earth oxide and B_2O_3 contents (by mol%) is possible.

4.2. The relations between NBO, compositions, and Ts

The relationships between T_s and NBO and the total alkaline earth oxide and B_2O_3 content are presented in Fig. 11 and, respectively. The relationship between T_s and NBO is similar to the relationship between CTE and NBO. With a constant B_2O_3 content, the T_s of glass decreases from 758 °C to 650 °C with an increase in the number of NBO. When the B_2O_3 content exceeds 20 mol%, again, no clear change was observed between NBO and T_s. Still, estimation of T_s by NBO with constant B_2O_3 content is possible. The relationship between T_s and the total alkaline earth oxide and B_2O_3 content

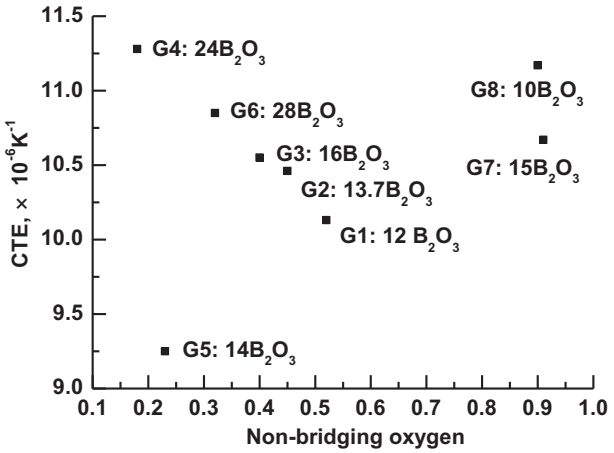

Fig. 9. The relation between the amount of NBO and CTE expansion in the BCSA system.

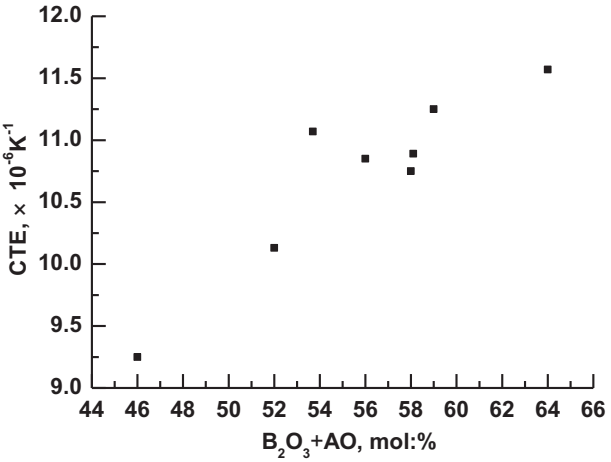

Fig. 10. The relation between the total alkaline earth oxide and B_2O_3 content (by mol%) and CTE in the BCSA system.

(Fig. 12) is rather clear. The T_s of glass decreases from 758 °C to 635 °C with the increase of content of alkaline earth oxides and B_2O_3, thus allowing one to estimate the T_s from the total alkaline earth oxide and B_2O_3 content (by mol%).

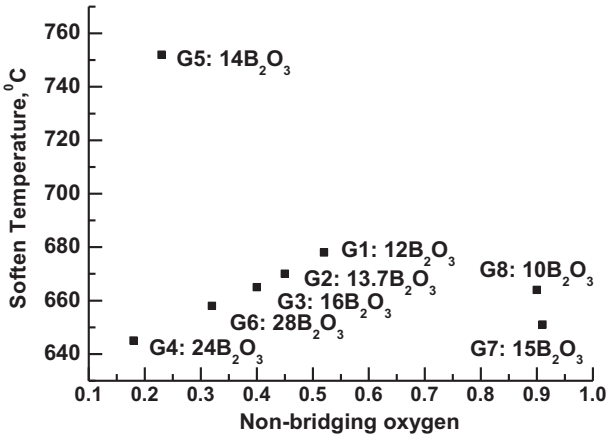

Fig. 11. The relationship between the amount of NBO and softening temperature of glass in the BCSA system.

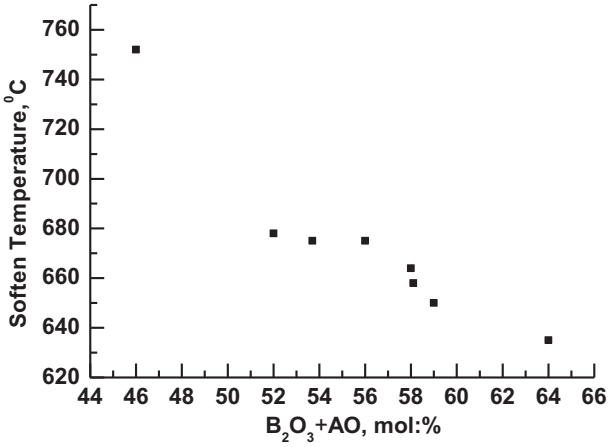

Fig. 12. The relation between the number of the total alkaline earth oxide and B_2O_3 content (by mol%) and softening temperature of glass in the BCSA system.

Several differences exist between the current results and those in literature [2,4–6]. First, previous literature reported that B_2O_3 needs to be added if a high CTE has to be achieved by glass formers. If the content exceeds 20 mol%, the "boron anomaly" occurs, and the T_s, T_g, and CTE of glass can also change correspondingly. The current results suggest that the "anomaly" phenomenon is not very clear for the properties of glass. The properties do not depend on a single parameter, such as the number of NBO, the content of B_2O_3, or Si/B. In the three glass systems, the alkaline earth oxide content has greater effect than B_2O_3 content on the properties of glass. Therefore, in the borosilicate glasses, if the glass contains alkaline earth oxides, the total alkaline earth oxide and B_2O_3 content should be a major parameter for the properties. Second, infrared spectra of glasses are a sensitive probe into the local structure of silicate glasses [14–18]; however, infrared spectral data for the borosilicate glass containing alkaline earth oxides are scarce. Bond energy has great impact on infrared absorption characteristics. The amount of NBOs in a silicate system can be reflected by the infrared absorption spectra [16]. The "effect of combined ions" weakens the attraction of the cation to the oxygen ions, thus decreasing the tetrahedral structure of BO_4. Hence, the disappearance or reduction of metaborate occurs in the SCSA glass systems and the BCSA glass system. Finally, previous literature reported that the SrO modifies glass properties, such as T_g, T_s and the CTE, but it cannot affect the wetting ability of glass. In the current experiment, however, the SrO can significantly improve the wetting ability of glass by decreasing the contact angle between the glass and crofer22 substrates, thus reducing the surface tension of molten glass in the SSA and SCSA glass systems and reducing the interfacial energy between the molten glass and crofer22 substrates. Therefore, SrO also determines adhesion/wetting with other SOFC/SOEC components.

5. Conclusions

Using prepared glasses based on $BaO–CaO–SiO_2–Al_2O_3$, $SrO–SiO_2–Al_2O_3$ and $SrO–CaO–SiO_2–Al_2O_3$, T_c of the seal glass with alkaline earth oxide has been found to increase in the order $BaO < SrO < CaO$.

In the BCSA system, with the decrease of ratio of Si/B from 3 to 1 and stable ratio of $M/F = 0.83$, the CTE of glass increases, and the T_s of glass decreases steadily. A direct relationship between the CTE and the total alkaline earth oxides and B_2O_3 content has also been found. B_2O_3 increases CTE of the glasses better than alkaline earth oxides. Moreover, the CTE and T_S increase directly with the field strength of alkaline earth cations in the order $Sr^{2+} < Ba^{2+} < Ca^{2+}$.

The optimum sealing temperature range of glass can be determined according to the $T_{sintering}$ and T_m of the parent glasses. Analysis of the contact angle between the glasses and crofer22 substrates indicates that G16 is the best option in sealing the SOECs/SOFCs under low loading without leakage; further, the SrO can improve the wetting ability of glass by decreasing the contact angle.

All the glasses fulfill the requirements for sealing the SOECs/SOFCs. The CTE of the BCSA system is closer to those of the interconnect and electrolyte. SrO-containing glasses show better wetting ability than other glasses; thus, they are the most suitable sealants for planar SOECs/SOFCs.

Acknowledgments

This work was supported as a Major Project of the National Science and Technology of China (Grant No. 2010ZX06901-020). We also gratefully acknowledge fundings from Tsinghua University (Contract No. 20101081790) and the State Key Laboratory of New Ceramics and Fine Processing (Grant No. 2010THZ08).

References

[1] Z. Yang, K.S. Weil, D.M. Paxton, J.W. Stevenson, J. Electrochem. Soc. 150 (2003) A1188.
[2] S.B. Sohn, S.Y. Choi, G.H. Kim, H.S. Song, G.D. Kim, J. Am. Ceram. Soc. 87 (2) (2004) 254.
[3] S.M. Gross, T. Koppitz, J. Remmel, J.B. Bouche, U. Reisgen, Full Cell Bull. (2006) 12.
[4] M.K. Mahapatra, K. Lu, Mater. Sci. Eng. R 67 (2010) 65.
[5] J.W. Fergus, J. Power Sources. 147 (2005) 46.
[6] J.H. Piao, K.N. Sun, N.Q. Zhang, D.R. Zhou, J. Hua, J. Synth. Crystals 33 (2004) 909.
[7] V.A.C. Haanappel, V. Shemet, I.C. Vinke, S.M. Gross, T.H. Koppitz, N.H. Menzler, M. Zahid, W.J. Quadakkers, J. Mater. Sci. 40 (2005) 1583.
[8] V.A.C. Haanappel, V. Shemet, I.C. Vinke, W.J. Quadakkers, J. Power Sources 141 (2005) 102.
[9] V. Kumar, A. Arora, O.P. Pandey, K. Singh, Int. J. Hydrogen Energy 33 (2008) 434.
[10] M.K. Mahapatra, K. Lu, J. Am. Ceram. Soc. 94 (3) (2011) 875.
[11] T. Jin, K. Lu, J. Power Sources 195 (2010) 4853.
[12] Y.S. Chou, J.W. Stevenson, P. Singh, J. Power Sources 184 (2008) 238.
[13] N. Laorodphan, P. Namwong, W. Thiemsorn, M. Jaimasith, A. Wannagon, T. Chairuangsri, J. Non-Cryst. Solids 355 (2009) 38.
[14] A. Goela, D.U. Tulyaganova, V.V. Khartona, A.A. Yaremchenkoa, S. Erikssonb, M.F. Ferreiraa, J. Power Sources 189 (2009) 1032–1043.
[15] A. Goel, D.U. Tulyaganov, A.M. Ferrari, E.R. Shaaban, A. Prange, F. Bondioliy, M.F. Ferreiraw, J. Am. Ceram. Soc. 93 (3) (2010) 830.
[16] K. Lua, M.K. Mahapatrab, J. Appl. Phys. 104 (2008) 074910.
[17] T.F. Soules, J. Chem. Phys. 71 (11) (1979) 4570.
[18] S.A. MacDonald, C.R. Schardt, D.J. Masiello, J.H. Simmons, J. Non-Cryst. Solids 275 (2000) 72.
[19] F.J. Shackelford, Ceramic and Glass Materials, Springer Science Business Media, LLC, MA, Boston, 2008.
[20] H. Bach, D. Krause (Eds.), Analysis of the Composition and Structure of Glass and Glass Ceramics, SpringerBerlin, New York, 1999.
[21] W.D. Kingery, H.K. Bowen, D.R. Uhlmann, Introduction to Ceramics, John Wiley and Sons, Inc., 1976.
[22] G.D. Chryssikos, M.S. Bitsis, J.A. Kapoutsis, E.I. Kamitsos, J. Non-Cryst. Solids 217 (1997) 278.
[23] F.H. El-Batal, E.M.A. Khalil, Y.M. Hamdy, H.M. Zidan, M.S. Aziz, A.M. Abdelghany, Physica B 405 (2010) 2648.
[24] G.D. Chryssikos, E.I. Kamitsos, A.P. Patsis, M.M. Bitsis, M.A. Karakassides, J. Non-Cryst. Solids 126 (1990) 42.
[25] R.E. Loehman, H.P. Dumm, H. Hofer, Ceram. Eng. Sci. Proc. 23 (2002) 699.